



## UvA-DARE (Digital Academic Repository)

### Plasma Assisted Catalytic Conversion of CO<sub>2</sub> and H<sub>2</sub>O Over Ni/Al<sub>2</sub>O<sub>3</sub> in a DBD Reactor

Ma, X.; Li, S.; Ronda-Lloret, M.; Chaudhary, R.; Lin, L.; van Rooij, G.; Gallucci, F.; Rothenberg, G.; Shiju, N. Raveendran; Hessel, V.

**DOI**

[10.1007/s11090-018-9931-1](https://doi.org/10.1007/s11090-018-9931-1)

**Publication date**

2019

**Document Version**

Final published version

**Published in**

Plasma Chemistry and Plasma Processing

**License**

CC BY

[Link to publication](#)

**Citation for published version (APA):**

Ma, X., Li, S., Ronda-Lloret, M., Chaudhary, R., Lin, L., van Rooij, G., Gallucci, F., Rothenberg, G., Shiju, N. R., & Hessel, V. (2019). Plasma Assisted Catalytic Conversion of CO<sub>2</sub> and H<sub>2</sub>O Over Ni/Al<sub>2</sub>O<sub>3</sub> in a DBD Reactor. *Plasma Chemistry and Plasma Processing*, 39(1), 109-124. <https://doi.org/10.1007/s11090-018-9931-1>

**General rights**

It is not permitted to download or to forward/distribute the text or part of it without the consent of the author(s) and/or copyright holder(s), other than for strictly personal, individual use, unless the work is under an open content license (like Creative Commons).

**Disclaimer/Complaints regulations**

If you believe that digital publication of certain material infringes any of your rights or (privacy) interests, please let the Library know, stating your reasons. In case of a legitimate complaint, the Library will make the material inaccessible and/or remove it from the website. Please Ask the Library: <https://uba.uva.nl/en/contact>, or a letter to: Library of the University of Amsterdam, Secretariat, Singel 425, 1012 WP Amsterdam, The Netherlands. You will be contacted as soon as possible.

*UvA-DARE is a service provided by the library of the University of Amsterdam (<https://dare.uva.nl>)*



# Plasma Assisted Catalytic Conversion of CO<sub>2</sub> and H<sub>2</sub>O Over Ni/Al<sub>2</sub>O<sub>3</sub> in a DBD Reactor

Xintong Ma<sup>1</sup> · Sirui Li<sup>1</sup> · Maria Ronda-Lloret<sup>2</sup> · Rohit Chaudhary<sup>1</sup> · Liangliang Lin<sup>1</sup> · Gerard van Rooij<sup>3</sup> · Fausto Gallucci<sup>1</sup> · Gadi Rothenberg<sup>2</sup> · N. Raveendran Shiju<sup>2</sup> · Volker Hessel<sup>1</sup>

Received: 26 April 2018 / Accepted: 23 September 2018 / Published online: 28 September 2018  
© The Author(s) 2018

## Abstract

We present an innovative approach for reacting carbon dioxide and water to give syngas by combining heterogeneous catalysis and non-thermal plasma techniques. This approach utilizes an abundant water and nickel catalyst, and mitigates the thermodynamic penalty by using a Dielectric Barrier Discharge (DBD) plasma reactor. Argon dilution was used in the experiment to reduce the exothermic recombination of hydrogen and oxygen, which is considered as the major hurdle for H<sub>2</sub>O conversion. As a result, the syngas ratio was dramatically improved from 0.07 to 0.86. In addition, the conversions of CO<sub>2</sub> and H<sub>2</sub>O were improved by packing Ni/γ-Al<sub>2</sub>O<sub>3</sub> catalysts into the DBD reactor. The yields of H<sub>2</sub> and CO were up to 13.8% and 5.6% respectively. The conditions for plasma catalysis and the catalyst characterization are presented and discussed.

**Keywords** Non-thermal plasma · Syngas production · CO<sub>2</sub> conversion

## Introduction

Global warming is a serious environmental issue that is exacerbated by the greenhouse effect. Mankind can work towards reducing this effect by decreasing the emission of anthropogenic greenhouse gases. Of these, CO<sub>2</sub> from fuel combustion is by far the largest, accounting for 72% of the total emissions [1]. According to the analysis by

---

**Electronic supplementary material** The online version of this article (<https://doi.org/10.1007/s11090-018-9931-1>) contains supplementary material, which is available to authorized users.

---

✉ Sirui Li  
S.Li1@tue.nl

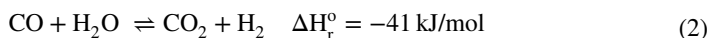
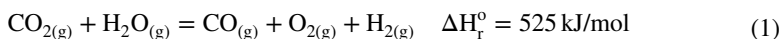
<sup>1</sup> Chemical Engineering and Chemistry Department, Eindhoven University of Technology, P.O. Box 513, 5600 MB Eindhoven, The Netherlands

<sup>2</sup> Van 't Hoff Institute for Molecular Sciences, University of Amsterdam, P.O. Box 94157, 1090GD Amsterdam, The Netherlands

<sup>3</sup> Dutch Institute for Fundamental Energy Research, P.O. Box 6336, 5600 HH Eindhoven, The Netherlands

the National Oceanic and Atmospheric Administration of the USA in 2016, the global annual temperature has increased at an average rate of 0.07 °C per decade since 1880 and at an average rate of 0.17 °C per decade since 1970 [2]. The atmospheric concentration of CO<sub>2</sub> keeps an upward tendency from 370 ppm in 2000 to 405 ppm in 2018 [3]. To control the concentration of CO<sub>2</sub> in the air, CO<sub>2</sub> capture and utilization could be one of the attractive solutions for the mitigation of CO<sub>2</sub> emissions.

Normally, hydrogen is used as co-reactant in the conventional CO<sub>2</sub> to fuel synthesis. H<sub>2</sub>O is not only a cheaper hydrogen source compared with H<sub>2</sub> and CH<sub>4</sub>, but also the common waste emitted with CO<sub>2</sub> in industrial processes such as ammonia production. The direct conversion of CO<sub>2</sub> and H<sub>2</sub>O is a promising approach based on the use of cheap, abundantly available raw materials.



However, converting CO<sub>2</sub> and H<sub>2</sub>O incurs a large thermodynamic penalty, requiring high temperature to break chemical bonds (1) due to the chemical stability of both components. This may be followed by a Water Gas Shift Reaction (WGSR) as shown in (2). Even at 2000 K, CO<sub>2</sub> conversion is only 1.5% [4]. Existing approaches for CO<sub>2</sub> and H<sub>2</sub>O conversion include electrolysis and photocatalysis, but they have various shortcomings such as high operation temperature in electrolysis [5] and low efficiency of solar energy utilization in photocatalysis [6]. Here, we turn to non-thermal plasma, which can be generated by electrical discharges at atmospheric pressure. It provides a way to convert CO<sub>2</sub> and H<sub>2</sub>O to syngas or hydrocarbons at low temperature and atmospheric pressure. Moreover, non-thermal plasma can be powered by electricity generated from renewable sources such as solar and wind, incorporating the CO<sub>2</sub> molecules into a renewable carbon cycle that can reduce the dependence on fossil fuels. In addition, this method is suitable decentralized and small-scale CO<sub>2</sub> conversion, which can be coupled to various CO<sub>2</sub> sources at suitable locations.

The conversion of CO<sub>2</sub> and H<sub>2</sub>O by non-thermal plasma was studied in DBD reactors [7, 8], microwave discharge reactors [9, 10], gliding arc discharge reactors [11], surface discharge reactors [12] and ferroelectric pellets packed-bed reactors [13]. However, the splitting of CO<sub>2</sub> and H<sub>2</sub>O molecules remains a challenge. The main product reported in those researches is syngas with different H<sub>2</sub>: CO ratios. Methane [8] and dimethyl ether [12] have also been observed, but not quantified. Guo et al. [9] studied the simultaneous dissociation of CO<sub>2</sub> and H<sub>2</sub>O in a surface wave sustained discharge operating at 915 MHz in a pulse regime, the highest yields of CO and H<sub>2</sub> are lower than 8% and 4%, respectively, at a flow rate of 6 slm. They added NiO/TiO<sub>2</sub> treated with Ar plasma in the CO<sub>2</sub> and H<sub>2</sub>O reaction to explore the synergy effect between plasma and catalysts. The conversion of CO<sub>2</sub> was improved from 23% (with plasma only) to 43%, with syngas as the sole product.

DBD is the discharge generated between two electrodes separated with an insulating barrier, which is widely applied in CO<sub>2</sub> conversion by non-thermal plasma [14]. Catalysts can be packed into the discharge zone of the DBD reactor and work with plasma synergistically. Ramses et al. [7] studied the conversion of CO<sub>2</sub> and H<sub>2</sub>O with H<sub>2</sub>O concentration in the feed gas from 0 to 8% in a DBD reactor. The conversions of CO<sub>2</sub> and H<sub>2</sub>O were <5% and syngas was produced with various H<sub>2</sub>/CO ratios up to 0.18. The ratio increased linearly with the increase of water content. Shaik et al. [8] reported that the CO<sub>2</sub> conversion ascends from 24% with plasma to 36% when combining the plasma with Ni/Al<sub>2</sub>O<sub>3</sub> catalysts. Carbon nanofibers were obtained in the packing region of the DBD reactor and CH<sub>4</sub> was detected besides syngas

in the product stream. However, the water conversion and the amount of methane produced were not mentioned in detail.

Our main aim here is to evaluate whether the addition of Ar and catalysts can increase the syngas ratios ( $H_2:CO$ ) and the conversions of  $CO_2$  and  $H_2O$ . First,  $CO_2$  and  $H_2O$  with various feed gas compositions were converted to syngas directly in the DBD reactor. Then, to improve the syngas ratio and  $H_2O$  conversion, different contents of Ar were added in the feed gases for the purpose of avoiding the recombination of  $H_2$  and  $O_2$ . Finally,  $Ni/\gamma-Al_2O_3$  catalysts were combined with plasma to improve the syngas ratios of the product stream and obtaining  $CH_4$ .

## Experimental

### Experimental Setup

The experiments are carried out in a cylindrical DBD reactor as shown in Fig. 1. A stainless-steel mesh (ground electrode) is wrapped over the outside of a quartz tube with outer and inner diameters of 13 mm and 10 mm, respectively (dielectric thickness = 1.5 mm). A stainless-steel rod with an outer diameter of 8 mm is placed in the center of the quartz tube and it acts as an inner electrode. The length of the discharge region is 100 mm with a discharge gap of 1 mm, which resulted in a discharge volume of  $2.83\text{ cm}^3$ . The inner electrode is connected to a high voltage output and the outer electrode is grounded via an external capacitor (100 nF). The DBD reactor is supplied by an AC high voltage–power supply (AFS generator G15S-150 K) for a maximum power of 1500 W, with a maximum peak-to-peak voltage of 60 kV and a frequency range of 10–150 kHz. The applied voltage ( $V_1$ ) is measured by a high voltage probe, while the voltage ( $V_2$ ) on the external capacitor is measured by another voltage probe. All of the electrical signals are measured by a four-channel digital oscilloscope. The Q–U Lissajous method is used to calculate the discharge power. The specific energy input (SEI) is equal to the ratio of the calculated discharge power to the gas flow, as in (3). The output products are detected by Gas Chromatography (Thermal Scientific Trace 1300) directly with Flame Ionization Detector (FID) for  $CH_4$  and Thermal Conductivity Detector (TCD) for other gases.

$$SEI [J\text{ cm}^{-3}] = \frac{\text{discharge power [W]}}{\text{flow rate [ml min}^{-1}]} \cdot \frac{60[s\text{ min}^{-1}]}{1[\text{cm}^3\text{ml}^{-1}]} \tag{3}$$

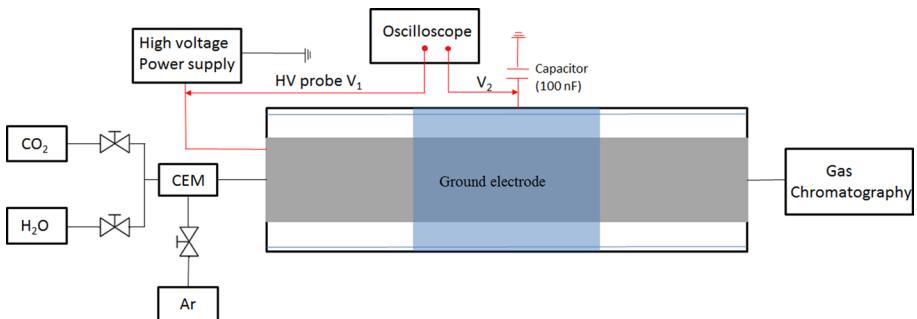


Fig. 1 Schematic diagram of the experimental setup

In the plasma catalytic section, the catalysts were fully packed into the discharge volume within the 1 mm gap. The reactions with CO<sub>2</sub> and H<sub>2</sub>O were carried out using plasma alone, plasma with support (Al<sub>2</sub>O<sub>3</sub>, TiO<sub>2</sub>) and plasma with catalysts (Ni/Al<sub>2</sub>O<sub>3</sub>) in the DBD reactor. The feeding gases, CO<sub>2</sub> and Ar were provided from gas cylinders and controlled by a set of mass flow controllers. H<sub>2</sub>O was evaporated and mixed with CO<sub>2</sub> in a controlled evaporator mixer. The gas line and the reactor were heated to 105 °C in order to avoid water condensation during reaction. The gas flow rates of CO<sub>2</sub>, H<sub>2</sub>O and Ar can be adjusted at ranges of 0–200 mL/min, 0–20 ml/min and 0–200 ml/min, respectively. The conversion, yield of CO<sub>2</sub> and H<sub>2</sub>O were calculated by comparing the CO<sub>2</sub> and H<sub>2</sub>O peak areas of the GC before and after plasma, processing based on following equations,

$$\text{CO}_2\text{conversion} [\%] = \frac{\text{moles of CO}_2\text{converted}}{\text{moles of CO}_2\text{in feed}} \cdot 100\% \quad (4)$$

$$\text{Yield of CO(H}_2\text{)} [\%] = \frac{\text{moles of CO(H}_2\text{)produced}}{\text{moles of CO}_2\text{(H}_2\text{O)in feed}} \cdot 100\% \quad (5)$$

To analyze the products, two different selectivities are defined, C-based selectivity for the C-containing species (e.g. CO, CH<sub>4</sub>) and the H-based selectivity for the H-containing species (e.g. CH<sub>4</sub>, H<sub>2</sub>).

H-based selectivity as Eqs. (6, 7):

$$S_{\text{H,H}_2} = \frac{\text{moles of H}_2\text{produced}}{\text{moles of H}_2\text{O consumed}} \quad (6)$$

$$S_{\text{H,CH}_4} = \frac{\text{moles of CH}_4\text{produced}}{\text{moles of H}_2\text{O consumed}} \cdot 2 \quad (7)$$

C-based selectivity as Eqs. (8, 9):

$$S_{\text{C,CO}} = \frac{\text{moles of CO produced}}{\text{moles of CO}_2\text{consumed}} \quad (8)$$

$$S_{\text{C,CH}_4} = \frac{\text{moles of CH}_4\text{produced}}{\text{moles of CO}_2\text{consumed}} \quad (9)$$

## Catalyst Preparation

Ni/ $\gamma$ -Al<sub>2</sub>O<sub>3</sub> catalysts were prepared by wet impregnation, using nickel nitrate hexahydrate Ni(NO<sub>3</sub>)<sub>2</sub>·6H<sub>2</sub>O, 98.5%, Sigma-Aldrich) as a Ni precursor and commercial Al<sub>2</sub>O<sub>3</sub> (Sigma-Aldrich) as support. The right amount of precursor was used to obtain 10, 20 and 30 wt% of metal loading. The formed slurry was stirred for 24 h at 60 °C, followed by 2-h drying at 120 °C and calcination in an open-air furnace at 450 °C for 4 h to obtain NiO/ $\gamma$ -Al<sub>2</sub>O<sub>3</sub>. Before the experiments, the catalysts were reduced in 20% H<sub>2</sub>/Ar flow with a flow rate of 30 ml/min at 700 °C for 1 h and are denoted as Ni/ $\gamma$ -Al<sub>2</sub>O<sub>3</sub>.

## Characterization of the Catalysts

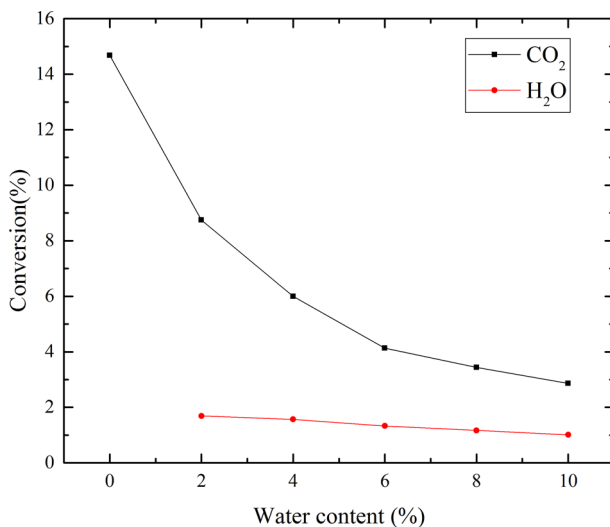
The following techniques were used to characterize the catalysts before and after the  $\text{CO}_2$  and  $\text{H}_2\text{O}$  reactions in the plasma-catalytic reactor. The surface area of the catalysts was determined by  $\text{N}_2$  adsorption at a  $-196^\circ\text{C}$ , using BET analysis. Temperature programmed reduction (TPR) was applied to check the reducibility of the catalysts. Before TPR measurements, the catalyst samples were heated in He at  $300^\circ\text{C}$  for 1 h and flushed with Ar for 1 h at  $50^\circ\text{C}$ . Afterwards, the sample was cooled down in flowing Ar to room temperature. The Ar flow was changed to 10%  $\text{H}_2/\text{Ar}$  and the reactor was heated linearly at a rate of  $10^\circ\text{C}/\text{min}$  up to  $900^\circ\text{C}$ . The  $\text{H}_2$  consumption was detected by a thermal conductivity detector (TCD). Analysis of the crystalline structure of the catalyst was conducted by X-ray Diffraction (XRD) at a scanning rate of  $0.02^\circ/20\text{ s}$  from  $2\theta$   $10^\circ$ – $90^\circ$ . The mass loss of the catalysts was measured by Thermogravimetric Analysis (TGA) in air by heating up to  $1000^\circ\text{C}$  at a rate of  $10^\circ\text{C}/\text{min}$ . Scanning Electron Microscopy (SEM) and Transmission Electron Microscopy (TEM) were used to observe the particle size of the catalysts and the structure of the samples.

## Results and Discussion

### Effect of $\text{H}_2\text{O}$ Content on the Conversion of $\text{CO}_2$ and $\text{H}_2\text{O}$

The impact of the  $\text{H}_2\text{O}$  content from 0 to 10% on the conversion of  $\text{CO}_2$  and  $\text{H}_2\text{O}$  was examined at a total rate of 100 ml/min in a blank DBD reactor as shown in Fig. 2. The operated voltage and frequency were 14 kV (from peak to peak) and 30 kHz respectively. The value of SEI was  $55.4\text{ J}/\text{cm}^3$  for all the reactions, which was calculated by integrating the area of Q–V Lissajous figure. As the concentration of  $\text{H}_2\text{O}$  increased, the conversion of  $\text{CO}_2$  decreased from 8.7 to 2.9% and the conversion of  $\text{H}_2\text{O}$  decreased slightly from 1.7 to 1.0%, as shown in Fig. 2.

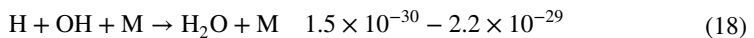
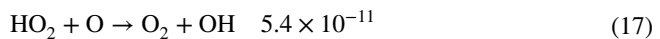
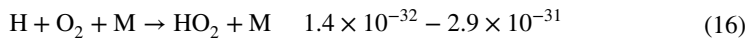
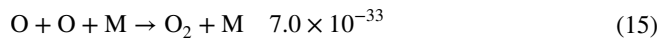
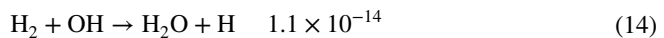
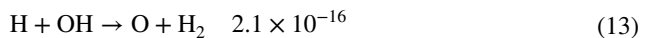
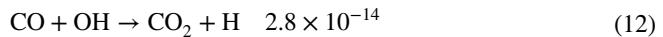
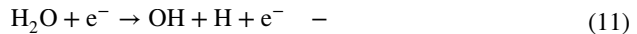
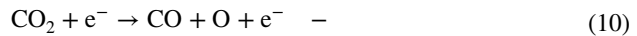
**Fig. 2**  $\text{CO}_2$  and  $\text{H}_2\text{O}$  conversion as a function of the water vapor content



The product compositions and syngas ratios are shown in Table 1. The main product is syngas with different H<sub>2</sub>/CO ratios. The addition of H<sub>2</sub>O led to a decline of the CO<sub>2</sub> conversion and an increase of H<sub>2</sub> production, resulting in a rise of syngas ratio in product, this is in line with reported literature [7, 11, 13]. In this way, the syngas ratio can be adjusted by changing the H<sub>2</sub>O/CO<sub>2</sub> ratio in the feed gases to fit the processing needs of gas fermentation. However, the current H<sub>2</sub>O conversion is less than 2% and the syngas ratio is too low to be applied in the industrial production.

There are two possible reasons for the low H<sub>2</sub>O conversion are as follows: (1) The addition of H<sub>2</sub>O vapor in the feed gas leads to a reduction in the number of micro-discharges [15] and electron density [7], resulting in low conversions of CO<sub>2</sub> and H<sub>2</sub>O [11]. (2) Rapid recombination reactions in plasma limit both of CO<sub>2</sub> and H<sub>2</sub>O feed gases conversions and syngas ratios in the product.

Rate coefficient  $k$  (cm<sup>3</sup> molecule<sup>-1</sup> s<sup>-1</sup>) [7]



The possible reaction path was listed as (10–18), the rate coefficient of related reactions was reported in a study of zero-dimension kinetic model by Ramses [7]. The formation of CO and H<sub>2</sub> are mainly through electron impact induced reaction (10) and (11). CO obtained from CO<sub>2</sub> dissociation can recombine with OH to form CO<sub>2</sub> rapidly and gives rise to the reduction of CO<sub>2</sub> conversion (12). This equation shows a higher reaction rate than the following reactions like H<sub>2</sub> production (13) and three body recombination of O<sub>2</sub>/H<sub>2</sub>O (15, 18), which was considered as the main reason leading to the low conversion of CO<sub>2</sub> [7]. The H atoms produced in Eqs. (11, 12) react further to generate H<sub>2</sub>, OH, H<sub>2</sub>O as

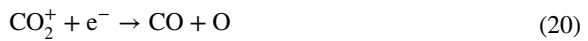
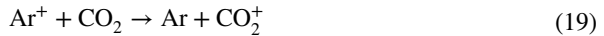
**Table 1** Product composition after plasma treatment

Water content (vol%)	CO (vol%)	H <sub>2</sub> (vol%)	O <sub>2</sub> (vol%)	H <sub>2</sub> /CO
0	14.3	0	7.6	0
2	8.6	0.03	4.6	0.003
4	5.9	0.06	3.3	0.01
6	4.0	0.09	2.3	0.02
8	3.2	0.09	2.0	0.03
10	1.9	0.1	1.1	0.05

Eqs. (13, 17) and react with OH back to H<sub>2</sub>O through three body recombination process (18), resulting in the low H<sub>2</sub>O conversion. Other species such as O<sub>3</sub> and H<sub>2</sub>O<sub>2</sub> can also form in theory, but analysing these is out of the scope of this paper.

### Effect of Ar on the Conversion of CO<sub>2</sub> and H<sub>2</sub>O

The conversion of CO<sub>2</sub> in DBD reactor rises dramatically with the addition of Ar [16]. The breakdown voltage is lower in the CO<sub>2</sub>/Ar mixtures owing to the higher Townsend ionization coefficient of Ar, this indicates that a larger fraction of the power can be utilized effectively for the CO<sub>2</sub> dissociation, as less power will be dissipated for the gas breakdown [16]. The charge could be transferred from the Ar<sup>+</sup> ions to CO<sub>2</sub>, which promotes the CO<sub>2</sub> splitting as shown in (19, 20). However, the ionisation of Ar requires a much higher electron energy (15.76 eV) than that for the excitation of Ar such as 11.55 eV for Ar (4s<sup>3</sup>P<sup>2</sup>), and 11.72 eV for Ar (4 s<sup>3</sup>P<sup>0</sup>) [17]. Thus, Ar is more likely excited to its metastable state rather than being ionized as given in the (21). The presence of the metastable Ar species (Ar\*) could create new reaction pathways for the dissociation of CO<sub>2</sub> as in (22) [18]. As H<sub>2</sub>O conversion was lower than 2% in the tests (Sect. 3.1), the effect of Ar was explored in the reaction to dilute the species generated in the reaction and avoid the recombination reactions.



The impact of the addition of 10%, 50% and 90% of Ar in the feed gases on the conversion of CO<sub>2</sub> and H<sub>2</sub>O was studied at a total rate of 100 ml/min in the DBD reactor as shown in Fig. 3. We could only test the H<sub>2</sub>O content up to 5% in 90% Ar, due to the limitation of the setup. The operated voltage and frequency were 14 kV (peak to peak) and 30 kHz, respectively. Generally, as the concentration of Ar increases, the conversion of H<sub>2</sub>O has an increasing tendency from 1 to 4.1%. However, the conversion of CO<sub>2</sub> decreased from 8.7

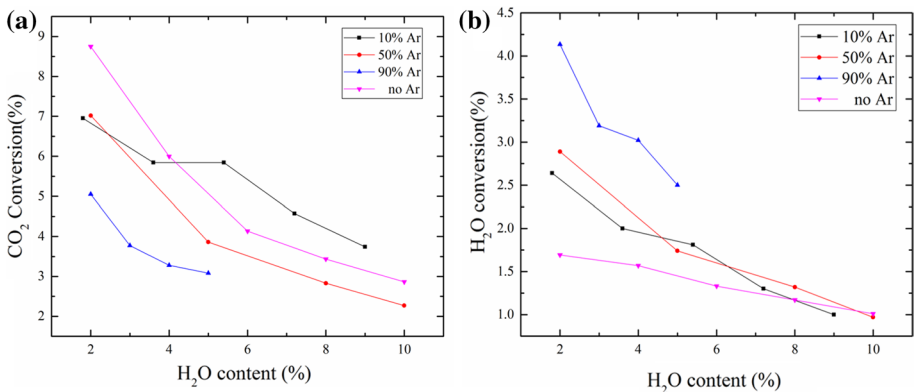


Fig. 3 The effect of Ar on the conversion of CO<sub>2</sub> (a) and H<sub>2</sub>O (b) at different H<sub>2</sub>O contents



to 3.1%. As for the tendency described in Sect. 3.1, the conversions of both  $\text{CO}_2$  and  $\text{H}_2\text{O}$  showed a decreasing trend with the rise of  $\text{H}_2\text{O}$  content. The products are syngas with various ratios. The values of SEI and syngas ratio are shown in Table 2.

Adding Ar promoted the conversion of  $\text{H}_2\text{O}$ , while the conversion of  $\text{CO}_2$  decreased simultaneously. The tendency is different from the effect of Ar on the conversion of  $\text{CO}_2$  alone [16]. The syngas ratios follow an upward tendency up to 0.86 with the increase of the  $\text{H}_2\text{O}$  content. The dissociation energy of  $\text{H}_2\text{O}$  (2.6 eV/mol) is slightly lower than that for the  $\text{CO}_2$  dissociation (2.9 eV/mol). Charge transfer between the reactive Ar species (e.g.  $\text{Ar}^*$ ,  $\text{Ar}^+$  ions) and  $\text{H}_2\text{O}$  might contribute to the  $\text{H}_2\text{O}$  dissociation. As a result, it promotes reverse reaction of  $\text{CO}_2$  leading to the decrease of the  $\text{CO}_2$  conversion. When the  $\text{H}_2\text{O}$  content is increased, the conversions of both  $\text{CO}_2$  and  $\text{H}_2\text{O}$  are decreased in all cases. The reason could be that the addition of  $\text{H}_2\text{O}$  leads to a reduction in electron density as discussed in Sect. 3.1.

### Catalytic Effect on the Conversion of $\text{CO}_2$ and $\text{H}_2\text{O}$ in the DBD Reactor

As summarized in the above discussion, both  $\text{H}_2\text{O}$  conversion and syngas ratio were enhanced with the addition of Ar. However, the conversion of  $\text{CO}_2$  and  $\text{H}_2\text{O}$  are still lower than 10%; besides, syngas ratio is slightly lower than the one for acetic acid production by Fischer–Tropsch synthesis. To improve the conversion and obtain hydrocarbons directly from the reaction, catalysts were packed into DBD reactor. Supported Ni catalysts were proved to enhance the conversions in  $\text{CO}_2$ – $\text{CH}_4$  dry reforming reaction by non-thermal plasma [19–22]. It also was used to improve the selectivity of  $\text{CH}_4$  for photocatalytic  $\text{CO}_2$  reduction by  $\text{H}_2\text{O}$  [23]. Thus, supported Ni catalysts were chosen as the catalysts in our experiments. The reaction with 90% Ar showed highest conversion of  $\text{H}_2\text{O}$ . Lower  $\text{H}_2\text{O}$  content supports the  $\text{CO}_2$  conversion, thus, the following experiments were performed with 90% Ar, 2%  $\text{H}_2\text{O}$  and 8%  $\text{CO}_2$ .

### Flow Rate Tests for Reaction

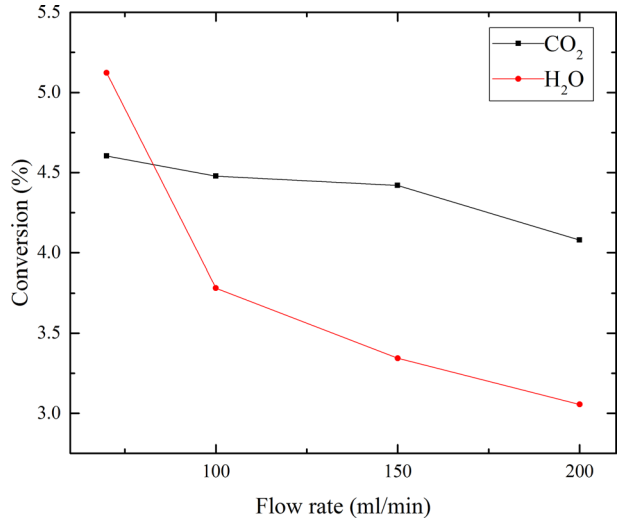
To study the effect of the flow rate on the reaction, 70 ml/min (lowest flow rate of the setup), 100 ml/min, 150 ml/min and 200 ml/min were applied in the plasma reaction. The operated voltage and frequency were 14 kV (from peak to peak) and 30 kHz, respectively. The conversions of  $\text{CO}_2$  and  $\text{H}_2\text{O}$  are shown in Fig. 4.

The conversions of feed gases showed a downward trend with a rise of total flow rate. The highest conversion of  $\text{CO}_2$  and  $\text{H}_2\text{O}$  was obtained at the lowest flow rate of 70 ml/min of feed gas. It coincides with the results in the  $\text{CO}_2$  dissociation [24] and  $\text{CO}_2$  hydrogenation in DBD reactor [25]. Low residence time leads to the low conversion of feed gases.

**Table 2** Specific energy input (SEI) values and syngas ratios in the product stream

Content of Ar in the feed gas %	SEI J/cm <sup>3</sup>	Syngas ratio
0	55.4	0.003–0.05
10	54.8	0.02–0.04
50	53.9	0.18–0.86
90	46.6	0.14–0.57

**Fig. 4** Conversion of CO<sub>2</sub> and H<sub>2</sub>O with various flow rates



Therefore, the optimal/lowest flow rate of 70 ml/min was selected for plasma catalytic experiments.

**Plasma Catalytic Reactions: Effect of  $\gamma$ -Al<sub>2</sub>O<sub>3</sub> and TiO<sub>2</sub>**

$\gamma$ -Al<sub>2</sub>O<sub>3</sub> and TiO<sub>2</sub> are the most common catalyst supports in plasma-catalytic reactions, which are chosen to compare the effects on the reaction resulting from various dielectric constants and specific surface areas. The first plasma-catalytic experiments were performed with these two supports. Experiment with blank reactor was also performed for comparison. The conversion of CO<sub>2</sub> and H<sub>2</sub>O as a function of time is presented in Fig. 5, and the Q–V Lissajous figures of these three cases are presented in Fig. 6. The operated voltage and frequency were 12 kV from peak to peak (the highest stable voltage for a long-term run) and 30 kHz in the reaction, respectively. Because Al<sub>2</sub>O<sub>3</sub> has a strong water absorption ability, product measurements were taken after 15 min of plasma treatment. In this way, the adsorbed water is released before the measurement so that the measurement results will not

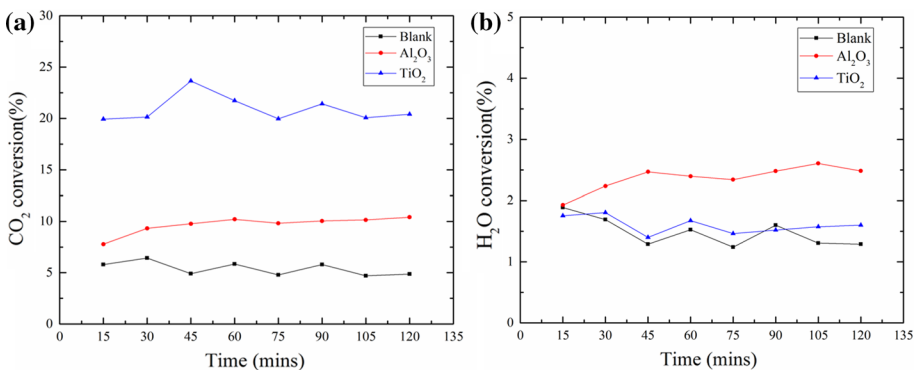
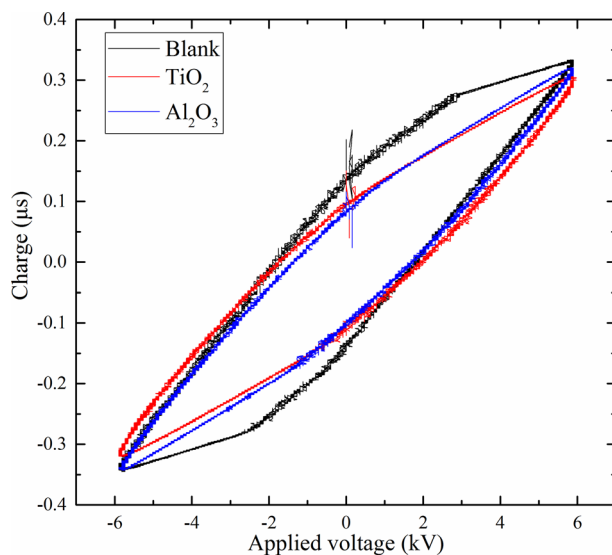


**Fig. 5** Conversion of CO<sub>2</sub> (a) and H<sub>2</sub>O (b) using different supports

**Fig. 6** Lissajous figures of reaction in DBD reactor without and with different packing material



be affected. The detected products were CO and H<sub>2</sub>. Figure 5 shows that TiO<sub>2</sub> was effectively enhanced CO<sub>2</sub> conversion, around 20–24% CO<sub>2</sub> conversion was achieved, which is 15% higher than the case when no catalyst is used. However, TiO<sub>2</sub> had no obvious effect on H<sub>2</sub>O conversion. The reaction with  $\gamma$ -Al<sub>2</sub>O<sub>3</sub> promotes CO<sub>2</sub> conversion from 5% (only plasma) to 10% and H<sub>2</sub>O conversion from 1.6 to 2.5%.

The shape of the Lissajous figure changes from parallelogram to oval shape when either TiO<sub>2</sub> or Al<sub>2</sub>O<sub>3</sub> are fully packed in the DBD reactor, resulting in the change of discharge mode from typical filamentary discharge to a combination of weak filamentary and predominantly surface discharge. The pellets fully packed into the discharge gap result in significant reduction in the discharge volume, limiting the distance where filamentary microdischarges can form [26]. As a result, less intense filament current peaks can be generated in the void between pellet–pellet and pellet–quartz wall as shown in Fig. S1. Meanwhile, a surface discharge can be formed on the surface of pellets near the contact points between the pellets, which is introduced as a packed-bed discharge effect [26, 27]. The breakdown voltage of the discharge does not change significantly with/without the packing materials from Fig. 6. The different discharge behaviors with packing pellets are caused by the enhanced local electric field strength near the contact points between the pellets and the pellet–dielectric wall [28]. From the measured V–I characteristics shown in Figure S1, differences in the number of microdischarges are observed with an order as: Blank > Al<sub>2</sub>O<sub>3</sub> > TiO<sub>2</sub>. In addition, the SEI in the case of TiO<sub>2</sub> is slightly higher than Al<sub>2</sub>O<sub>3</sub> (29.3 J/cm<sup>3</sup> and 25.8 J/cm<sup>3</sup> respectively), which could also contribute to the difference in conversion of CO<sub>2</sub>. The difference in discharge characteristics between Al<sub>2</sub>O<sub>3</sub> and TiO<sub>2</sub> is not significant. We believe that the main reason for the difference in conversion is the physical properties of the packing material. The surface area of TiO<sub>2</sub> is much smaller than Al<sub>2</sub>O<sub>3</sub> (Table S3). Indeed the plasma generation in micropores is less likely to occur, however, Al<sub>2</sub>O<sub>3</sub> with large surface area and strong H<sub>2</sub>O absorption capacity can absorb more H<sub>2</sub>O on the surface compared with TiO<sub>2</sub> at the same flow rate, leading to higher residence time of H<sub>2</sub>O on the surface of pellets which promotes the H<sub>2</sub> production. At the same time more OH is produced, which will react with CO, resulting in a lower conversion of CO<sub>2</sub>.

On the other hand, the rate of CO reverse reactions is mainly determined by the surface rather than the gas phase. Therefore,  $\text{TiO}_2$  with lower surface area gives a lower rate for CO to react with oxygen species, hence higher  $\text{CO}_2$  conversion is observed [29].

Since  $\gamma\text{-Al}_2\text{O}_3$  showed the best  $\text{H}_2\text{O}$  conversion results, it was used as the support for the following experiments. The introduction of  $\text{Ni}/\gamma\text{-Al}_2\text{O}_3$  catalysts in the plasma discharge was reported to improve the performance of  $\text{CO}_2$  activation reactions with hydrocarbons or with  $\text{H}_2\text{O}$ , in comparison with the plasma-only reaction [8, 30, 31]. Thus,  $\text{Ni}/\gamma\text{-Al}_2\text{O}_3$  was used to explore the catalytic effect on this reaction further.

### Plasma Catalytic Reactions: Effect of $\text{Ni}/\gamma\text{-Al}_2\text{O}_3$ on the Conversion of $\text{CO}_2$ and $\text{H}_2\text{O}$

To study the effect of different metal loadings on the catalytic activity, 10%  $\text{Ni}/\text{Al}_2\text{O}_3$ , 20%  $\text{Ni}/\text{Al}_2\text{O}_3$  and 30%  $\text{Ni}/\text{Al}_2\text{O}_3$  catalysts were studied and compared with blank experiments. The results are presented in Fig. 7.

From Fig. 7, 10%  $\text{Ni}/\text{Al}_2\text{O}_3$  significantly showed a positive effect on the conversion of  $\text{CO}_2$ , converting between 10 and 14% of  $\text{CO}_2$  and showing the best  $\text{CO}_2$  conversion results compared with the others in 2-h reaction. It also has slightly higher conversion of  $\text{H}_2\text{O}$  compared with the blank and  $\text{Al}_2\text{O}_3$ .  $\text{CO}_2$  conversion with 30%  $\text{Ni}/\text{Al}_2\text{O}_3$  catalyst was similar to  $\text{Al}_2\text{O}_3$ , while  $\text{H}_2\text{O}$  conversion was slightly higher. It is evident that 20%  $\text{Ni}/\text{Al}_2\text{O}_3$  shows the lowest  $\text{CO}_2$  conversion values compared with other conditions. However, it is the most active for  $\text{H}_2\text{O}$  conversion. Although the conversion declines from 14.7 to 4% after 120 min, these values are always higher than the  $\text{H}_2\text{O}$  conversions in the other cases.

Furthermore, the products in all cases were syngas with different ratios, apart from 292 ppm  $\text{CH}_4$  obtained with 20%  $\text{Ni}/\text{Al}_2\text{O}_3$ .  $\text{H}_2$  and CO yields were up to 13.8% and 5.6%, respectively (Fig. 8).  $\text{CH}_4$  achieved the highest yield 0.32% at 15 min of reaction (first measurement) and it was not produced anymore after 75 min of reaction. The highest syngas ratio was 0.6 after 15 min due to the high yield of  $\text{H}_2$ , and it decreased to 0.2 after 2 h of reaction. Thus, metallic Ni is more active than NiO for  $\text{H}_2\text{O}$  conversion, and it can produce  $\text{CH}_4$  from Figs. 8 and 9.

The C-based selectivity and H-based selectivity are depicted in Fig. 9. The C-based selectivity of  $\text{CH}_4$  decreased from 7 to 0% with time. Reversely, the selectivity of CO increased from 93 to 100% after 75 min of reaction. Besides, the maximum value of H-based  $\text{CH}_4$  selectivity was 11%, descending with reaction time.

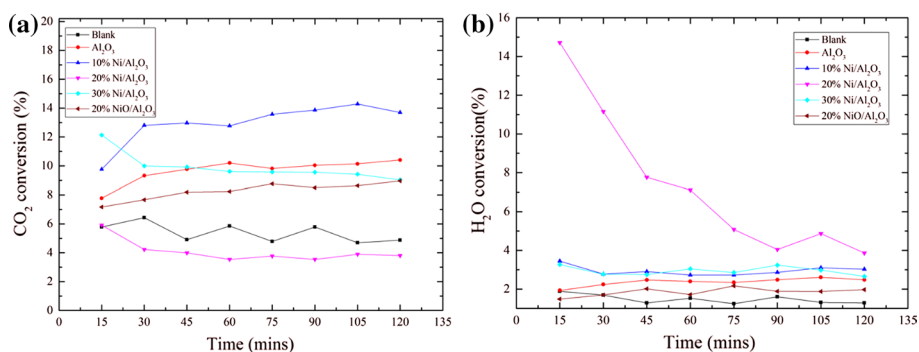


**Fig. 7** Conversion of  $\text{CO}_2$  (a) and  $\text{H}_2\text{O}$  (b) with no catalyst,  $\text{Al}_2\text{O}_3$ , 10%  $\text{Ni}/\text{Al}_2\text{O}_3$ , 20%  $\text{Ni}/\text{Al}_2\text{O}_3$ , 30%  $\text{Ni}/\text{Al}_2\text{O}_3$  and 20%  $\text{NiO}/\text{Al}_2\text{O}_3$

**Fig. 8** Yield of valuable products in the reaction using 20% Ni/Al<sub>2</sub>O<sub>3</sub> catalyst

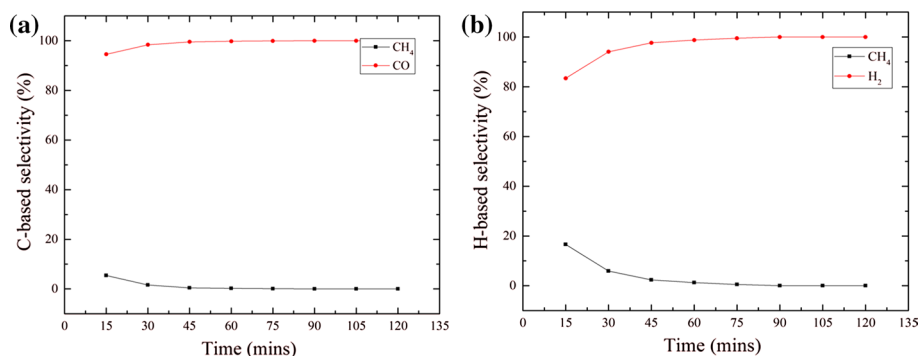
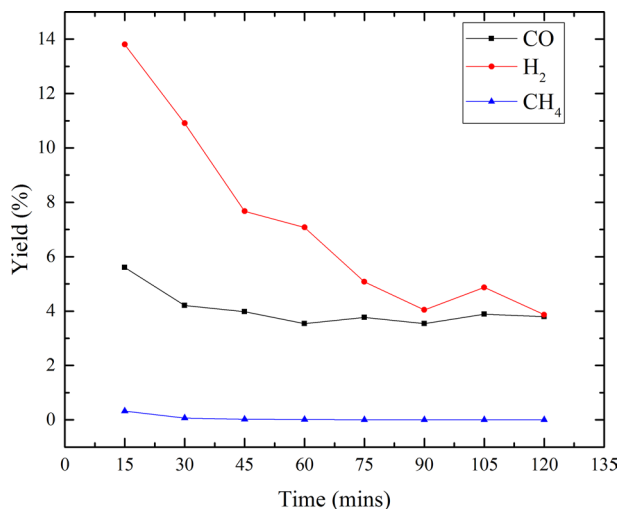


**Fig. 9** Selectivity of valuable products in the reaction with 20% Ni/Al<sub>2</sub>O<sub>3</sub>

The ability of Ni/Al<sub>2</sub>O<sub>3</sub> to increase CO<sub>2</sub> conversion was observed previously [8], which is in accordance with results of 10% Ni/Al<sub>2</sub>O<sub>3</sub>. However, Ni/Al<sub>2</sub>O<sub>3</sub> catalysts are also active for the Water Gas Shift (WGS) reaction (2) [32], which could explain the catalytic behavior of 20% Ni/Al<sub>2</sub>O<sub>3</sub> catalyst. The CO produced from CO<sub>2</sub> dissociation could react with H<sub>2</sub>O, promoting the production of H<sub>2</sub> and CO<sub>2</sub> by the WGS reaction. However, the conversion decreased with time in 90 min. One possible explanation for this behavior is that CO dissociated to C (Boudouard reaction), reducing the conversion of H<sub>2</sub>O. This carbon can react with H<sub>2</sub> further to produce CH<sub>4</sub>, as shown in Fig. 10 [18]. When the H<sub>2</sub> concentration in the product mixture decreased, CH<sub>4</sub> production decreased to zero in an hour. It was also reported that CO<sub>2</sub> by in situ formation of hydrogen during water splitting with Ni catalysts may result in the production of CH<sub>4</sub> and PCVD of CH<sub>4</sub>, leading to the formation of carbon fibers in a DBD reactor [8]. Because CH<sub>4</sub> was detected during the 20% Ni/Al<sub>2</sub>O<sub>3</sub> reaction, so the other possible reason is that the formation of carbon filaments from the PCVD of CH<sub>4</sub> may reduce the catalyst activity and H<sub>2</sub> production.

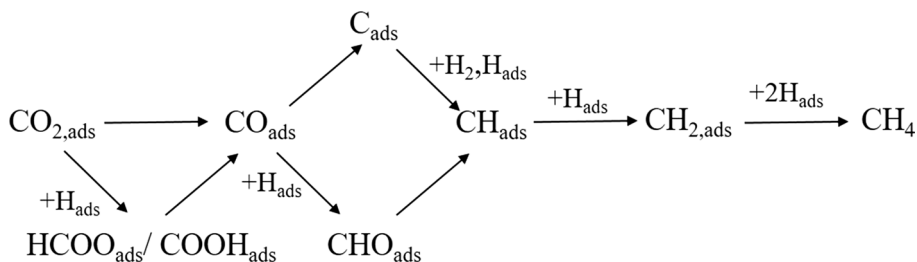


**Fig. 10** Possible major reactions for the formation of  $\text{CH}_4$  on the  $\text{Ni}/\text{Al}_2\text{O}_3$  catalyst. Reprinted with permission from [18], copyright 2017 Springer

To conclude, we have seen that inserting packing materials in the DBD plasma discharge can enhance the conversions compared with plasma alone. 10%  $\text{Ni}/\text{Al}_2\text{O}_3$  shows the best  $\text{CO}_2$  conversion (14%) but less significant for  $\text{H}_2\text{O}$  conversion. On the other hand, the reaction with 20%  $\text{Ni}/\text{Al}_2\text{O}_3$  catalyst present much higher  $\text{H}_2\text{O}$  conversion (14.7%) and lower  $\text{CO}_2$  conversion (5.9%) compared with 10%  $\text{Ni}/\text{Al}_2\text{O}_3$ , suggesting 20%  $\text{Ni}/\text{Al}_2\text{O}_3$  is more effective for side reactions (WGS) and promotes  $\text{H}_2$  production. Further, the  $\text{CO}_2$  conversion of 20%  $\text{Ni}/\text{Al}_2\text{O}_3$  reaction is lower than that in blank experiments, indicating that the WGS reaction occurs during 20%  $\text{Ni}/\text{Al}_2\text{O}_3$  reactions and reduces  $\text{CO}$  production. Unlike 20%  $\text{Ni}/\text{Al}_2\text{O}_3$ , all the  $\text{CO}_2$  and  $\text{H}_2\text{O}$  conversions in other cases were enhanced compared with blank experiments, suggesting that the dissociation reactions of  $\text{CO}_2$  and  $\text{H}_2\text{O}$  to  $\text{CO}$  and  $\text{H}_2$  play a dominating role. Besides, it is also possible that  $\text{Ni}$  reacts with  $\text{H}_2\text{O}$  to produce  $\text{NiO}$  and  $\text{H}_2$  ( $\text{Ni} + \text{H}_2\text{O} = \text{NiO} + \text{H}_2$ ) during the reaction and increases the  $\text{H}_2$  production at the beginning of reaction with 20%  $\text{Ni}$ . The experiments with 30%  $\text{Ni}$  gave low conversions, suggesting the thermal catalysis and sintering may occur especially in the case of 30%  $\text{Ni}/\text{Al}_2\text{O}_3$ . Further characterization of the materials was performed to study the observed catalytic behavior.

## Catalysts Characterization

### X-ray Diffraction (XRD) Measurements

The XRD patterns for the 10%  $\text{Ni}/\text{Al}_2\text{O}_3$ , 20%  $\text{Ni}/\text{Al}_2\text{O}_3$ , 30%  $\text{Ni}/\text{Al}_2\text{O}_3$  catalysts after reduction and after reaction are shown in Fig. S6. The characteristic peaks of  $\text{NiO}$  are not obvious in 10%/20%  $\text{Ni}$  and absent from the 30% $\text{Ni}$  sample. Therefore, it cannot be confirmed that  $\text{NiO}$  formation is the dominating factor. The  $\text{Ni}$  peak of 30%  $\text{Ni}/\text{Al}_2\text{O}_3$  after reaction is more intense than the peak before reaction unlike peaks of 10%/20%  $\text{Ni}/\text{Al}_2\text{O}_3$ . The average crystallite size of  $\text{Ni}$  in 30%  $\text{Ni}/\text{Al}_2\text{O}_3$  catalyst was estimated by the Scherrer formula using the half width of the  $\text{Ni}$  (200) peak, which was 16.5 nm after reduction and 25.3 nm after reaction. This shows that sintering of  $\text{Ni}$  particles takes place during the reaction with 30%  $\text{Ni}/\text{Al}_2\text{O}_3$ .

### Transmission Electron Microscopy (TEM) and Scanning Electron Microscopy (SEM) Analysis

TEM and SEM analysis of the catalysts after reduction (noted as before reaction) and after reaction were performed in order to study the formation of carbon deposits. Compared

with the clean surface of reduced Ni/Al<sub>2</sub>O<sub>3</sub> samples (before reaction) shown in Fig. S7. (a, c, e) from SEM images, filamentary deposits were clearly present on the surface of the catalysts after their use in the reaction for 2 h [Fig. S7. (b, d, f)]. This carbon can be identified as filamentary carbon [33, 34]. With TEM images, the amount of carbon filaments in 10% Ni/Al<sub>2</sub>O<sub>3</sub> catalyst is small, making it difficult to identify. From Fig. S7 (a, b), the carbon filaments are not encapsulating the particles, therefore they do not influence the catalytic activity of this material. For 20% Ni/Al<sub>2</sub>O<sub>3</sub>, more carbon filaments are observed [Fig. S8 (c, d)]. They stay closer to the metal clusters, causing partial encapsulation. Fig. S8 (e, f) clearly shows that the carbon formed on the surface of 30% Ni/Al<sub>2</sub>O<sub>3</sub> catalyst is encapsulating the metal particles. Curiously, those filaments form a V shape. Deactivation of the Ni catalysts by coking is a common problem [35, 36]. Coking can be produced from two different reactions: the Boudouard reaction ( $2\text{CO} \rightarrow \text{CO}_2 + \text{C}$ ) and/or the hydrocarbon decomposition. It is possible that CH<sub>4</sub> is produced, but it decomposes to C and H<sub>2</sub>.

In summary, the amount of metal loading strongly affects the properties of the final catalysts. 30% Ni/Al<sub>2</sub>O<sub>3</sub> catalyst has bigger metal clusters with a weak interaction with the support (Fig. S5) and a significantly lower surface area than the other two materials (Table. S3), which may be the main reason for its poor catalytic activity. Besides, temperature gradients at the catalyst surface in DBD reactor may arise and influence the overall catalyst activity [37]. The heat capacity of metals Ni ( $C_p = 0.44 \text{ J g}^{-1} \text{ K}^{-1}$ ) is typically lower than the heat capacity of most commonly dielectric support materials Al<sub>2</sub>O<sub>3</sub> ( $C_p = 0.72 \text{ J g}^{-1} \text{ K}^{-1}$ ) while the thermal conductivity of metals is much higher ( $\kappa = 90.9 \text{ W m}^{-1} \text{ K}^{-1}$  for Ni,  $\kappa = 20 \text{ W m}^{-1} \text{ K}^{-1}$  for Al<sub>2</sub>O<sub>3</sub>) [37]. Therefore, the temperature will be higher in the Ni surface in the plasma reaction leading to the sintering and deactivation of catalysts especially for 30% Ni/Al<sub>2</sub>O<sub>3</sub>. Moreover, it induces the formation of encapsulating carbon filaments that block the active sites. For 20% Ni/Al<sub>2</sub>O<sub>3</sub> catalyst, it is the least active material for CO<sub>2</sub> conversion, but the best catalyst for H<sub>2</sub>O conversion. This behavior may reflect the presence of side reactions such as WGS reaction, methane formation/PCVD and Ni oxidation as explained in Sect. 3.3.3. But Ni oxidation to NiO was not obvious from XRD, suggesting that reducing species such as hydrogen and CO produced in the plasma may react with NiO and reduce it. Among the studied materials, 10% metal loading appeared to be the best one for CO<sub>2</sub> conversion, although it could not convert H<sub>2</sub>O. Characterization results (Fig. S5) showed that 10% Ni/Al<sub>2</sub>O<sub>3</sub> catalyst contains highly dispersed NiO nanoparticles with a strong interaction with the support, giving a material with a high surface area. In this case the metal-support interface can adsorb more CO<sub>2</sub>, while the formation of carbon filaments is partially avoided.

## Conclusions

The conversion of CO<sub>2</sub> and H<sub>2</sub>O was carried out in a DBD plasma reactor at 105 °C. The effects of argon addition, packed support material and supported catalysts were studied. The addition of Ar produces reactive Ar species and reduces the recombination of H<sub>2</sub> and O<sub>2</sub>, which promotes the H<sub>2</sub>O conversion. In this case, the syngas ratio can be adjusted to 0–0.86, which approaches the ratio for hydrocarbon synthesis via Fischer–Tropsch synthesis or gas fermentation. Further, the plasma catalytic CO<sub>2</sub> and H<sub>2</sub>O reaction was explored with Ni/Al<sub>2</sub>O<sub>3</sub> catalyst to improve the conversion of feed gases and to give access to hydrocarbons. Thus, the combination of plasma and a 10% Ni/Al<sub>2</sub>O<sub>3</sub> catalyst facilitates the CO<sub>2</sub> conversion. The 20% Ni/Al<sub>2</sub>O<sub>3</sub> catalyst promotes the water–gas shift reaction (WGS) and

enhances the H<sub>2</sub>O conversion up to 14.7%. In addition, 292 ppm CH<sub>4</sub> was obtained by the plasma reaction, which assumed to be formed from CO through dissociation and hydrogenation. The effect of the 30% Ni/Al<sub>2</sub>O<sub>3</sub> catalyst is similar to Al<sub>2</sub>O<sub>3</sub> as packing material which is accounted to sintering of the catalyst and carbon deposition.

**Acknowledgements** The authors acknowledge the technical assistance of Carlo Buijs (SEM, TEM) and Marco Hendrix (XRD) from Chemical Reactor Engineering Section and Physical Chemistry Section of Chemical Engineering and Chemistry Department, Eindhoven University of Technology. The authors also acknowledge the support from Chinese Scholarship Council (CSC).

**Open Access** This article is distributed under the terms of the Creative Commons Attribution 4.0 International License (<http://creativecommons.org/licenses/by/4.0/>), which permits unrestricted use, distribution, and reproduction in any medium, provided you give appropriate credit to the original author(s) and the source, provide a link to the Creative Commons license, and indicate if changes were made.

## References

1. <http://timeforchange.org/CO2-cause-of-global-warming>. Accessed 9 Aug 2018
2. NOAA National Centers for Environmental Information (2017) State of the climate: global climate report for annual 2016. <https://www.ncdc.noaa.gov/sotc/global/201613>. Accessed 9 Aug 2018
3. <https://www.CO2.earth/>. Accessed 9 Aug 2018
4. Snoeckx R, Bogaerts A (2017) Plasma technology: a novel solution for CO<sub>2</sub> conversion? *Chem Soc Rev* 46:5805–5863
5. Chen X, Guan C, Xiao G, Du X, Wang J-Q (2015) Syngas production by high temperature steam/CO<sub>2</sub> coelectrolysis using solid oxide electrolysis cells. *Faraday Discuss* 182:341–351
6. Li K, An X, Park KH, Khraisheh M, Tang J (2014) A critical review of CO<sub>2</sub> photoconversion: catalysts and reactors. *Catal Today* 224:3–12
7. Snoeckx R, Ozkan A, Reniers F, Bogaerts A (2016) The quest for value-added products from CO<sub>2</sub> and H<sub>2</sub>O in a dielectric barrier discharge: a chemical kinetics study. *Chemsuschem* 10(2):409–424
8. Mahammadunnisa S, Reddy EL, Ray D, Subrahmanyam C, Whitehead JC (2013) CO<sub>2</sub> reduction to syngas and carbon nanofibres by plasma-assisted in situ decomposition of water. *Int J Greenh Gas Control* 16(1):361–363
9. Chen G et al (2015) Simultaneous dissociation of CO<sub>2</sub> and H<sub>2</sub>O to syngas in a surface-wave microwave discharge. *Int J Hydrog Energy* 40(9):3789–3796
10. Chen G, Godfroid T, Britun N, Georgieva V, Delplancke-Ogletree MP, Snyders R (2017) Plasma-catalytic conversion of CO<sub>2</sub> and CO<sub>2</sub>/H<sub>2</sub>O in a surface-wave sustained microwave discharge. *Appl Catal B Environ* 214:114–125
11. Indarto A, Yang DR, Choi JW, Lee H, Song HK (2007) Gliding arc plasma processing of CO<sub>2</sub> conversion. *J Hazard Mater* 146(1–2):309–315
12. Hayashi N, Yamakawa T, Baba S (2006) Effect of additive gases on synthesis of organic compounds from carbon dioxide using non-thermal plasma produced by atmospheric surface discharges. *Vacuum* 80(11–12):1299–1304
13. Futamura S, Kabashima H (2004) Synthesis gas production from CO<sub>2</sub> and H<sub>2</sub>O with nonthermal plasma. *Stud Surf Sci Catal* 153:119–124
14. Brandenburg R (2017) Dielectric barrier discharges: progress on plasma sources and on the understanding of regimes and single filaments. *Plasma Sourc Sci Technol* 26:053001
15. Zhang X, Lee BJ, Im HG, Cha MS (2016) Ozone production with dielectric barrier discharge: effects of power source and humidity. *IEEE Trans Plasma Sci* 44(10):2288–2296
16. Ramakers M, Michielsen I, Aerts R, Meynen V, Bogaerts A (2015) Effect of argon or helium on the CO<sub>2</sub> conversion in a dielectric barrier discharge. *Plasma Process Polym* 12:755–763
17. Sadeghi N, Setser DW, Touzeau M (2002) Reactions of metastable argon atoms with molecular hydrogen at 300 and 80 K: origin of the ultraviolet chemiluminescence. *J Phys Chem A* 106(36):8399–8405
18. Zeng Y, Tu X (2017) Plasma-catalytic hydrogenation of CO<sub>2</sub> for the cogeneration of CO and CH<sub>4</sub> in a dielectric barrier discharge reactor: effect of argon addition. *J Phys D Appl Phys* 50:184004
19. Wang S, Lu GQM (1998) CO<sub>2</sub> reforming of methane on Ni catalysts: effects of the support phase and preparation technique. *Appl Catal B Environ* 16(3):269–277



20. Juan-Juan J, Román-Martínez MC, Illán-Gómez MJ (2004) Catalytic activity and characterization of Ni/Al<sub>2</sub>O<sub>3</sub> and NiK/Al<sub>2</sub>O<sub>3</sub> catalysts for CO<sub>2</sub> methane reforming. *Appl Catal A Gen* 264(2):169–174
21. Guo J, Lou H, Zhao H, Chai D, Zheng X (2004) Dry reforming of methane over nickel catalysts supported on magnesium aluminate spinels. *Appl Catal A Gen* 273(1–2):75–82
22. Pompeo F, Nichio NN, González MG, Montes M (2005) Characterization of Ni/SiO<sub>2</sub> and Ni/Li–SiO<sub>2</sub> catalysts for methane dry reforming. *Catal Today* 107–108:856–862
23. Tahir M, Tahir B, Amin NAS, Muhammad A (2016) Photocatalytic CO<sub>2</sub> methanation over NiO/In<sub>2</sub>O<sub>3</sub> promoted TiO<sub>2</sub> nanocatalysts using H<sub>2</sub>O and/or H<sub>2</sub> reductants. *Energy Convers Manag* 119:368–378
24. Mei D, He Y, Liu S, Yan J, Tu X (2016) Optimization of CO<sub>2</sub> conversion in a cylindrical dielectric barrier discharge reactor using design of experiments. *Plasma Process Polym* 13(5):544–556
25. Eliasson B, Kogelschatz U, Xue B, Zhou L-M (1998) Hydrogenation of carbon dioxide to methanol with a discharge-activated catalyst. *Ind Eng Chem Res* 37(8):3350–3357
26. Tu X, Gallon HJ, Twigg MV, Gorry PA, Whitehead JC (2011) Dry reforming of methane over a Ni/Al<sub>2</sub>O<sub>3</sub> catalyst in a coaxial dielectric barrier discharge reactor. *J Phys D Appl Phys* 44(27):274007
27. Kim H-H, Kim J-H, Ogata A (2009) Microscopic observation of discharge plasma on the surface of zeolites supported metal nanoparticles. *J Phys D Appl Phys* 42(13):135210
28. Butterworth T, Allen RWK (2017) Plasma-catalyst interaction studied in a single pellet DBD reactor: dielectric constant effect on plasma dynamics. *Plasma Sourc Sci Technol* 26(6):065008
29. Banerjee AM, Billinger J, Nordheden K, Peeters FJJ (2018) Conversion of CO<sub>2</sub> in a packed-bed dielectric barrier discharge reactor. *J Vac Sci Technol A* 36:04F403
30. Mahammadunnisa S, Manoj Kumar Reddy P, Ramaraju B, Subrahmanyam C (2013) Catalytic non-thermal plasma reactor for dry reforming of methane. *Energy Fuels* 27(8):4441–4447
31. Tu X, Whitehead JC (2012) Plasma-catalytic dry reforming of methane in an atmospheric dielectric barrier discharge: understanding the synergistic effect at low temperature. *Appl Catal B Environ* 125:439–448
32. Haryanto A, Fernando SD, To SDF, Steele PH, Pordesimo L, Adhikar S (2011) High temperature water gas shift reaction over nickel catalysts for hydrogen production: effect of supports, GHSV, metal loading, and dopant materials. *J Pharmacogenomics Pharmacoproteomics* 2:106. <https://doi.org/10.4172/2157-7544.1000106>
33. You X et al (2014) Ni–Co/Al<sub>2</sub>O<sub>3</sub> bimetallic catalysts for CH<sub>4</sub> steam reforming: elucidating the role of Co for improving coke resistance. *ChemCatChem* 6(12):3377–3386
34. Zhu X, Huo P, Zhang YP, Cheng DG, Liu CJ (2008) Structure and reactivity of plasma treated Ni/Al<sub>2</sub>O<sub>3</sub> catalyst for CO<sub>2</sub> reforming of methane. *Appl Catal B Environ* 81(1–2):132–140
35. Joo OS, Jung KD (2002) CH<sub>4</sub> dry reforming on alumina-supported nickel catalyst. *Bull Korean Chem Soc* 23(8):1149–1153
36. Al-Fatish ASA, Ibrahim AA, Fakeeha AH, Soliman MA, Siddiqui MRH, Abasaeed AE (2009) Coke formation during CO<sub>2</sub> reforming of CH<sub>4</sub> over alumina-supported nickel catalysts. *Appl Catal A Gen* 364(1–2):150–155
37. Neyts EC (2016) Plasma-surface interactions in plasma catalysis. *Plasma Chem Plasma Process* 36(1):185–212